FFT-OT: A Fast Algorithm for Optimal Transportation

Na Lei[*1] and Xianfeng Gu[2]

[1]Dalian University of Technology
[2]Stony Brook University

Abstract

An optimal transportation map finds the most economical way to transport one probability measure to the other. It has been applied in a broad range of applications in vision, deep learning and medical images. By Brenier theory, computing the optimal transport map is equivalent to solving a Monge-Ampère equation. Due to the highly non-linear nature, the computation of optimal transportation maps in large scale is very challenging.

This work proposes a simple but powerful method, the FFT-OT algorithm, to tackle this difficulty based on three key ideas. First, solving Monge-Ampère equation is converted to a fixed point problem; Second, the obliqueness property of optimal transportation maps are reformulated as Neumann boundary conditions on rectangular domains; Third, FFT is applied in each iteration to solve a Poisson equation in order to improve the efficiency.

Experiments on surfaces captured from 3D scanning and reconstructed from medical imaging are conducted, and compared with other existing methods. Our experimental results show that the proposed FFT-OT algorithm is simple, general and scalable with high efficiency and accuracy.

1. Introduction

Recent years have witnessed the rapid development of optimal transportation and its broad applications in vision [32, 31, 41, 38], deep learning [1, 16, 28] and medical imaging [18, 17, 39, 29]. An *optimal transportation map* (OT map) finds the most economical way to transport one probability measure to the other, the total transportation cost is treated as the *Wasserstein distance* between the two random distributions. Therefore, OT maps have been used for measuring the differences among probability distributions, and for registering images or 3D shapes.

Motivation Due to the highly non-linear nature, improving the computational efficiency of OT maps becomes one of the central challenges. Researchers have developed

---
*Corresponding author

many methods to tackle this difficult problem with different emphasises. For examples, the Sinkhorn algorithm [35, 7, 25, 12] greatly improves the optimization speed of the Kantorovich potential by adding an entropy regularizer terms, but sacrificing the accuracy; the convex geometric variational algorithms [39, 24, 27] find the precise solution, but with complex dynamic geometric data structure and adaptive arithmetic precision. The fluid dynamic algorithms [2, 19, 18] find the optimal flow in space-time, therefore increases the dimension and reduces the computational efficiency.Therefore, existing methods can hardly find the accurate solutions for large scale OT problems efficiently.

In order to handle the challenge, this work proposes a novel algorithm: FFT-OT, which computes large scale optimal transportation maps with high efficiency and accuracy using the fundamental and powerful tool: Fast Fourier Transformation.

Key Ideas The proposed algorithm is based on three simple ideas. The goal is to find the OT map between two probability measures $T : (\Omega, fdx) \to (\Omega^*, gdy)$, based on Brenier's theorem 3.1, this is reduced to finding the Brenier potential $u : \Omega \to \mathbb{R}$ by solving the Monge-Ampere equation (1).

1. Fixed point By improving the formulation in [10, 4], an operator in the Sobolev space is constructed $\mathcal{P} : H^2(\Omega) \to H^2(\Omega)$, such that the solution u^* of the Monge-Ampere equation is the fixed point of $\mathcal{P}$, $\mathcal{P}[u^*] = u^*$. The fixed point can be achieved by iterations, $u^{(n+1)} \leftarrow \mathcal{P}[u^{(n)}]$, when $n \to \infty$, $u^{(n)}$ converges to u^*, $u^{(n)} \to u^*$. The convergence of the iteration process and the convexity of the solution has theoretic guarantees.

2. Obliqueness Boundary Condition The boundary condition $Du(\Omega) = \Omega^*$ is difficult to directly formulated. Our formulation is based on the obliqueness boundary condition in Eqn. (5). Suppose the domain Ω is a planar rectangle, the Brenier potential is rewritten as

$$u(x, y) = (x^2 + y^2)/2 + \varphi,$$

where $-\varphi$ is the well-known Kantorovich potential. The obliqueness condition is equivalent to the Neumann bound-

ary conditon $\partial\varphi/\partial\mathbf{n} = 0$ of the Kantorovich potential φ.

3. Fast Fourier Transformation During the fixed point iterations, the operator $\mathcal{P}[u^{(n)}]$ is to solve a Poisson equation Eqn. (4) and Eqn. (6). Since the domain has a natural regular grid structure, it is very convenient to use finite difference method to solve the Poisson equation [36]. More crucially, since the discrete Laplace matrix has the fixed structure, the Poisson equation can be solved using the FFT method to reduces the complexity.

Contributions This work proposes a simple FFT-OT algorithm to solve the OT problem by the classical FFT method.

Advantages The simple FFT-OT algorithm greatly improves the computational efficiency, accuracy and scalability. It can be implemented on GPU or FPGAs to further improve the speed. Furthermore, it can be directly generalized to higher dimensional situations. So the proposed FFT-OT algorithm has great potential to handle large scale real time OT problems.

Disadvantages The proposed FFT-OT algorithm requires the supports of the probability distributions to be rectangular. Nevertheless, it is possible to generalize the algorithm to general convex domains. The proposed FFT-OT algorithm focuses on 2 dimensional cases only, but it can be generalized to higher dimensional situations.

2. Related Work

There is a vast literature on optimal transportation problem. For a thorough review, we refer the readers to [43, 44] for theories and [30] for computational methods. In the following we will briefly review the most related works. The existing algorithms can be roughly classified into four categories:

Kantorovich Formulation Monge-Kantorovich theory has been applied to solve optimal transportation problem via linear programming technique [20, 21]. Karmarkar proposed a polynomial time algorithm for linear programming in [22]. Sinkhorn proposed to add an entropy regularizer term to approximate the solution with high efficiency [35]. Recently, many algorithms based on the Sinkhorn algorithm are proposed. These methods firstly add an entropic regularizer to the prime Kantorovich formulation, and then solve either its prime problem [7, 25] or the dual problem [12]. Genevay et al. [12] proposed stochastic optimization for Kantorovich potential with entropic regularization to handle large-scale OT problems. In theory, this type of algorithms can only give approximations.

Brenier Formulation Gu et.al [15] built the theoretical connection between the Brenier theorem and Alexandrov theorem in convex geometry. Su et.al. proposed a geometric variational approach to solve optimal transport maps in [47] for surface area-preserving mapping, in [40] for cortical surface matching and in [39] for surface registration. Levy

generalized the method for volumetric cases in [24, 23]. The method has been generalized to register surfaces with more complicated topologies, in [48], multiply-connected surface registration in [37]. De Goes et al. [9] proposed to use OT for 2D shape reconstruction and simplification, later on they generalized to use capacity-constrained Voronoi tessellation to deal with blue noise processing problem [8]. Mérigot [27] proposed a multi-scale approach to accelerate the computation for large scale problems. Seguy et al. [34] proposed a regularization relaxation of OT problem and approximated the Alexandrov potential with DNN. The method are also generalized to the spherical OT maps in [29, 45] and [6], where the power diagrams are constructed on the sphere. These methods compute the Brenier potential using power diagrams, which require sophisticated geometric data structures and adaptive arithmetic.

Fluid Dynamics Benamou-Brenier reformulated the optimal transportation using fluid dynamics [2] . A flow starting from the source density and ending at the target density with minimal kinetic energy induces a family of time dependent diffeomorphisms, the final diffeomorphism is the desired OT map with L^2 cost. The theorem leads to a robust algorithm [19]. Haker, Angenenent and Tannenbaum proposed a method in [18] to improve a measure-preserving map by removing the divergence free component. Haber, Rehman and Tannenbaum further improved the efficiency of the method in [17] and applied for volumetric medical imaging. These methods solve the OT problem in time-space domain, increase the time and storage complexity.

Direct Numerical Methods There are many numerical algorithms for solving Monge-Ampere equation by different linearization methods. a) Loeper and Rapetti introduced the linearization of Monge-Ampere based on the derivative of matrix determinant in [26], which focuses on uniform target density. Saumier, Agueh and Khouider [33] generalized the method to non-uniform target densities and combined with Strain's spectral method [36] to compute OT maps for image processing. During the iteration, each step is reduced to solve a variant coefficient Poisson equation, and special step-length is carefully chosen to ensure the convergence; b) Dean and Glowinski [10] linearized the Monge-Ampere equation using the algebraic identity 2 and compute the OT map by least square method. Benamou, Frosse and Oberman generalized the method to higher dimensions in [4]. c) Georges and Guennebaud [13] introduced a different linearization method and used finite difference method to solve the OT problem. Their method is restricted on 2D with unform target density only, and the Poisson equation formulation is difficult to utilize FFT directly.

Comparison Comparing with methods in Kantorovich formulation, such as Sinkhorn [35], our proposed algorithm finds the solution with high accuracy, the approximation error is $O(h^2)$, where h is the spacial step length [5]; Com-
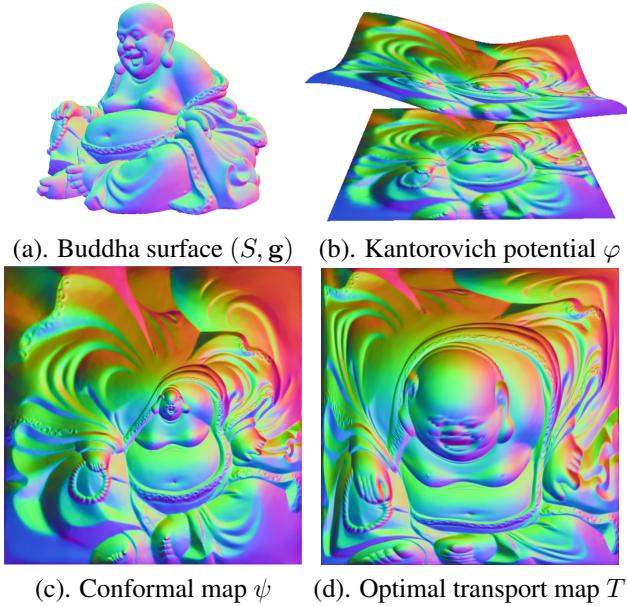
(a). Buddha surface $(S, \mathbf{g})$ (b). Kantorovich potential φ

(c). Conformal map ψ (d). Optimal transport map T

Figure 1: The Buddha example demonstrates the Brenier's theorem, computed by the FFT-OT algorithm 2.

paring with methods of computing Brenier potential using geoemtric optimization, such as [39], our algorithm doesn't require complex data structure, therefore greatly simplifies the design and improves the efficiency; comparing with the most direct numerical methods, our algorithm use FFT to solve Poisson equations, therefore is much simpler and faster.

3. Basic Concepts and Theorems

The fundamental concepts and theorems are briefly reviewed, more details can be found in [43].

Monge's Problem Given two probability distributions $f(x)dx$ and $g(y)dy$ with supports Ω and Ω^* respectively. A C^1 map $T : \Omega \to \Omega^*$ is *measure preserving* if $\det DT(x) = f(x)/g \circ T(x)$, where DT is the *Jacobian* of the map, and denoted as $T_\# f = g$. Given a *cost* function $c : \Omega \times \Omega^* \to \mathbb{R}$ representing the cost for transporting a unit mass from point x to y, the *transport cost* of the mapping T is defined as $\mathcal{C}(T) := \int_\Omega c(x, T(x)) f(x) dx$. Monge raised the problem to find the *optimal transport map*, which is the measure preserving map with the least transportation cost,

$$\min\{\mathcal{C}(T) : T : \Omega \to \Omega^*, T_\# f = g\}.$$

Brenier's Theorem The Brenier's theorem gives an answer to Monge's problem, under mild regularity conditions:

Theorem 3.1 (Brenier). *If the transport cost is the quadratic Euclidean distance, $c(x, y) = \frac{1}{2}|x - y|^2$, then there exists a convex function $u : \Omega \to \mathbb{R}$, unique up to a constant, such that the gradient map $T = Du : \Omega \to \Omega^*$*
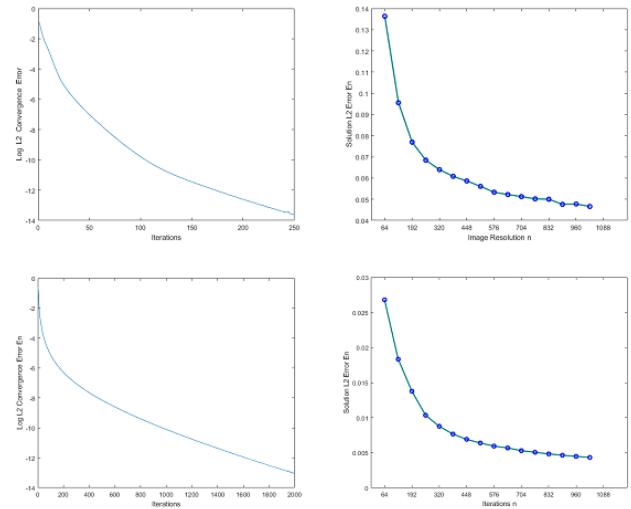

Figure 2: Convergence Rate and Accuracy Test. Top row: Buddha surface; bottom row: brain cortical surface. Resolution $1k \times 1k$, $\varepsilon = 1e - 15$. Left: the convergence error during the iterations; right: the solution L^2 error with respect to the resolution.

is the unique optimal transport map. u is called the Brenier potential, satisfying the Monge-Ampère *equation:*

$$\det D^2 u(x) = \frac{f(x)}{g \circ Du(x)}, \tag{1}$$

with the boundary condition: $Du(\Omega) = \Omega^*$.

Fig. 1 illustrates the theorem, computed using the FFT-OT algorithm 2. Frame (a) shows the Buddha surface $(S, \mathbf{g})$ in $\mathbb{R}^3$, with a metric $\mathbf{g}$. Assume after normalization, the total surface area is 1. Frame (c) shows the conformal map $\psi : S \to \Omega$, where Ω is the unit square. ψ push-forwards surface area element $dA_{\mathbf{g}}$ to the plane. Frame (d) shows the OT map $T : (\Omega, \psi_\# dA_{\mathbf{g}}) \to (\Omega, \mathcal{L})$, where $\mathcal{L}$ is the Lebesgue's measure. Frame (b) shows the Kantorovich potential $\varphi = u - (x^2 + y^2)/2$, where u is the Brenier potential and $T = Du$.

Obliqueness Boundary Condition General OT maps satisfy the obqliueness condition [42].

Lemma 3.2 (Obliqueness). *Suppose $\Omega, \Omega^* \subset \mathbb{R}^n$ are bounded domains, Ω is convex, $\partial\Omega^*$ is C^1. The density functions f and g satsify the balance condition $\int_\Omega f = \int_{\Omega^*} g$, and are bounded, $0 < c_0 < f, g < c_1 < \infty$, the Brenier potential is $u : \Omega \to \mathbb{R}$. Suppose $x \in \partial\Omega$ and $q \in \partial\Omega^*$, $Du(x) = y$, then $\langle \mathbf{n}(x), \mathbf{n}(y) \rangle > 0$, where $\mathbf{n}$ represents the inner normal.*

4. Computational Algorithm

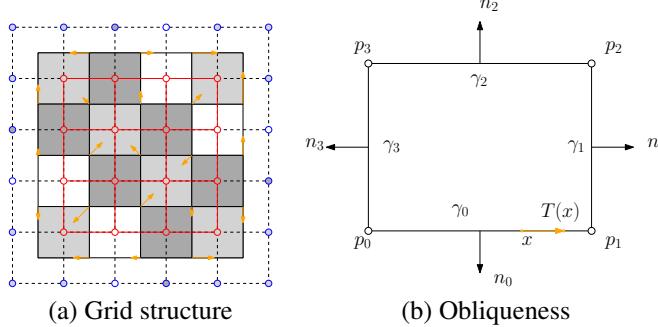The Monge-Ampère equation (1) is highly non-linear, therefore difficult to solve directly. Our key idea is to con-

(a) Grid structure   (b) Obliqueness

Figure 3: The sample nodes (red) and the gohst nodes (blue) are in the cell centers. The obliqueness condition is equivalent to the Neumann boundry condition.

vert the OT problem to a fixed point problem and solve it using FFT.

Fixed Point In two dimensional case, the Monge-Ampère equation can be written as $u_{xx}u_{yy} - u_{xy}^2 = f/g \circ Du$. Therefore

$$(u_{xx} + u_{yy})^2 = u_{xx}^2 + u_{yy}^2 + 2u_{xy}^2 + 2\frac{f}{g \circ Du}, \quad (2)$$

this leads to a Poisson equation,

$$\Delta u = \sqrt{u_{xx}^2 + u_{yy}^2 + 2u_{xy}^2 + 2f/g \circ Du}, \quad (3)$$

where $\Delta = \partial^2/\partial x^2 + \partial^2/\partial y^2$. Because the Brenier potential is convex, its Laplacian is non-negative, hence we take the positive square root in the above formula. This ensures the convexity of the Brenier potential during the computational process [3]. We define the operator $\mathcal{T} : H^2(\Omega) \to H^2(\Omega)$,

$$\mathcal{T}[u] = \Delta^{-1}\left\{\sqrt{u_{xx}^2 + u_{yy}^2 + 2u_{xy}^2 + 2f/g \circ Du}\right\} \quad (4)$$

The solution to the Monge-Ampère equation 1 is the fixed point u^* of $\mathcal{T}$, $\mathcal{T}(u^*) = u^*$. Therefore, we can search for the fixed point by iterative method, $u^{(n+1)} = T[u^{(n)}]$, the convergence is proved in [10, 4].

Obliqueness Condition In the current work, we focus on rectangular planar domain, namely $\Omega = \Omega^* = [-1, +1] \times [-1, +1]$. As shown in Fig. 3, the four corner points p_k's divide the boundary into four segments γ_k, $k = 0, 1, 2, 3$. The normal to γ_k is $\mathbf{n}_k$. Given a boundary point $x \in \gamma_k$, its image is also a boundary point $T(x) \in \partial\Omega^*$. By obliqueness lemma 3.2, we have $\langle \mathbf{n}(x), \mathbf{n}(T(x)) \rangle > 0$, therefore

$$\mathbf{n}(x) = \mathbf{n}(T(x)), \quad (5)$$

therefore $T(x)$ is also on γ_k, namely both x and $T(x)$ are on the same γ_k. Since each corner point belongs to 2 adjacent segments, therefore its image is itself, $T(p_k) = p_k$. Let $u(x, y) = \varphi(x, y) + (x^2 + y^2)/2$, φ be the *Kantorovich*

potential. We obtain $Du = D\varphi + \text{Id}$ and $\Delta u = \Delta\varphi + 2$. The operator $\mathcal{T}[u]$ in Eqn. (4) is converted to the operator $\mathcal{P}[\varphi]$ in Eqn. (6). The obliqueness condition (5) becomes to the Neumann boundary condition, namely $\partial\varphi/\mathbf{n} = 0$.

Finite Difference Method As shown in figure 3, the image domain Ω^* is discretized to a Cartesian $M \times N$ grid. The step lengths are given by $h_x = 2/M$ and $h_y = 2/N$. The coordinates of each grid point are given by $(x_i, y_i) = \left(-1 + \frac{h_x}{2} + ih_x, -1 + \frac{h_y}{2} + jh_y\right)$. We add "ghost cells" to the boundary as shown in figure 3 frame (a) in order to evaluate high order derivatives for the Neumann boundary condition. The Brenier potential is represented as a two dimensional $M \times N$ matrix (u_{ij}), the differentials are approximated by the central difference method,

$$\mathcal{D}_{xx}^2 u_{ij} = \frac{1}{h_x^2}(u_{i+1,j} + u_{i-1,j} - 2u_{i,j})$$
$$\mathcal{D}_{yy}^2 u_{ij} = \frac{1}{h_y^2}(u_{i,j+1} + u_{i,j-1} - 2u_{i,j})$$
$$\mathcal{D}_{xy}^2 u_{ij} = \frac{1}{4h_x h_y}(u_{i+1,j+1} + u_{i-1,j-1} \quad (7)$$
$$- u_{i-1,j+1} - u_{i+1,j-1})$$

The discrete Laplace matrix has a canonical form (see the supplementary document), the regular structure allows us to apply FFT method to speed up the computation.

bf FFT to solve Poisson Equation Suppose we are given a Poisson equation $\Delta u = \rho$ with Neumann boundary condition $\partial u/\mathbf{n} = 0$, the necessary condition for the existence of a solution can be derived as follows:

$$\int_\Omega \rho = \int_\Omega \Delta u = \int_\Omega \nabla \cdot \nabla u = \int_{\partial\Omega} \frac{\partial u}{\partial \mathbf{n}} ds = 0. \quad (8)$$

If ρ doesn't satisfy the condition, we can add an offset c to ρ, such that the integration of $\rho - c$ is 0. For solving discrete Poisson equation

$$u_{i+1,j} + u_{i-1,j} + u_{i,j+1} + u_{i,j-1} - 4u_{ij} = \rho_{i,j}, \quad (9)$$

with Neumann boundary condition, we can use the Discrete Cosine Transformation (DCT) method. Given two dimensional array $u(i, j)$, the two dimensional DCT is given by

$$\tilde{u}(m, n) = c(m, n) \sum_{i,j} u(i, j) \cos\frac{(2i+1)m\pi}{2M} \cos\frac{(2j+1)n\pi}{2N},$$

and the inverse DCT is

$$u(i, j) = \sum_{m,n} c(m, n)\tilde{u}(m, n) \cos\frac{(2i+1)m\pi}{2M} \cos\frac{(2j+1)n\pi}{2N},$$

where $m, i = 0, 1, \ldots, M - 1$ and $n, j = 0, 1, \ldots, N - 1$,

$$c(m, n) = \begin{cases} \frac{\sqrt{2}}{\sqrt{MN}} & m = 0, n = 0 \\ \frac{2}{\sqrt{MN}} & \text{otherwise} \end{cases}$$

Let $\tilde{\rho} = \text{DCT}(\rho)$, the solution to the discrete Poisson equation (9) is u, $\tilde{u} = \text{DCT}(u)$, then it can be easily proved that

$$\tilde{u}(m, n) = \frac{\tilde{\rho}(m, n)}{2[\cos\frac{m\pi}{M} + \cos\frac{n\pi}{N} - 2]}. \quad (10)$$

$$\mathcal{P}\left[\varphi^{(n)}\right] := \Delta^{-1}\rho^{(n)} = \Delta^{-1}\left\{\sqrt{\left[\varphi_{xx}^{(n)}+1\right]^2 + \left[\varphi_{yy}^{(n)}+1\right]^2 + 2\left[\varphi_{xy}^{(n)}\right]^2 + 2f/g \circ \left[Id + D\varphi^{(n)}\right]} - 2\right\}. \quad (6)$$

The solution is unique upto a constant. By setting $\tilde{u}(0,0)$ to be zero, we can normalize the solution. DCT and inverse DCT can be computed using the Fast Fourier Transform (FFT) method efficiently. The algorithm to solve the discrete Poisson equation with Neumann boundary condition is summarized in Alg. (1).

Algorithm 1: DCT Poisson Equation Solver

Input: Matrix $\rho(i,j)$ on the rectangular grid,
$\quad (i,j) \in \{0,1,\ldots,M-1\} \times \{0,1,\ldots,N-1\}$
Output: Solution to $\Delta u = \rho$, s.t. $\partial u/\partial \mathbf{n} = 0$.
Add an offset to ρ such that Eqn. (8) holds;
Use FFT to compute DCT $\tilde{\rho} = \text{DCT}(\rho)$;
Compute $\tilde{u}$ using Eqn. (10);
Use FFT to compute the inverse DCT $u = \text{IDCT}(\tilde{u})$.

Monge-Ampère Equation Solver Solving the Monge-Ampère equation (1) is reduced to find the fixed point of the operator $\mathcal{P}$ in Eqn. (6), which can be obtained by iterations $\varphi^{(n+1)} \leftarrow \mathcal{P}[\varphi^{(n)}]$. At teach iteration step, evaluating $\mathcal{P}[\varphi^{(n)}]$ is equivalent to solving a Poisson equation.

At the beginning, the Brenier potential is set to be $u^{(0)} = (x^2 + y^2)/2$, $\varphi^{(0)}$ zero everywhere, and the OT map $T^{(0)}$ is the identity map. In each iteration, we copy $\varphi^{(n)}$ of each ghost cell from its closest regular cell in order to ensure the Neumann boundary condition. We compute $\varphi_{xx}^{(n)}$, $\varphi_{yy}^{(n)}$, $\varphi_{xy}^{(n)}$, $_x^{(n)}$ and $\varphi_y^{(n)}$ using the finite difference operators (7), then evaluate the operator $\mathcal{P}[\varphi^{(n)}]$ using Eqn. (6). In order to evaluate $g \circ [Id + \nabla\varphi^{(n)}]$, we convert the grid to a quad-mesh, the (i,j)-th vertex position is defined as $[Id + D\varphi^{(n)}](x_i, y_j)$. Then we render the mesh to cover the domain Ω using the density g as the color. The rendering can be obtained either by the scan conversion algorithm [14] on CPU or use GPU directly. Once the right hand side of Poisson equation (6) is obtained, we can solve the equation using the DCT-Poisson equation solver (1), and update $\varphi^{(n+1)} \leftarrow \mathcal{P}[\varphi^{(n)}]$. We repeat this process until the L^2 distance between $\varphi^{(n)}$ and $\varphi^{(n+1)}$ is less than a prescribed threshold ε. The algorithm is summarized in Alg. (2). Fig 4 shows the process for the OT map from a Gaussian distribution to the Lebesgue's measure $\mathcal{L}$. The top row shows the Kantorovich potential $\varphi^{(n)}$, the bottom row the intermediate mappings $Id + D\varphi^{(n)}$.

Algorithm 2: FFT-OT

Input: Source density $f(i,j)$ and target density
$\quad g(i,j)$ defined on $\Omega = [-1,1] \times [-1,1]$,
$\quad (i,j) \in \{0,\ldots,M-1\} \times \{0,\ldots,N-1\}$;
$\quad$ a convergence threshold $\varepsilon > 0$
. **Output:** The optimal transport map
$\quad Du : (\Omega, f) \rightarrow (\Omega, g)$
Initialize $\varphi^{(0)} \leftarrow 0$;
while *true* **do**
$\quad$ Set the ghost cells by copying $\phi^{(n)}$ from the
$\quad$ closest normal cells;
$\quad$ Compute $\phi_x^{(n)}$ and $\phi_y^{(n)}$ and compute
$\quad g \circ [Id + D\varphi^{(n)}]$ using scan conversion;
$\quad$ Compute $\phi_{xx}^{(n)}$, $\phi_{yy}^{(n)}$ and $\phi_{xy}^{(n)}$ using Eqn. (7);
$\quad$ Compute the right hand side $\rho^{(n)}$ of Eqn. (6);
$\quad$ Solve discrete Poisson equation
$\quad \Delta\phi^{(n+1)} = \rho^{(n)}$ using Alg. (1);
$\quad$ Update $\varphi^{(n+1)} \leftarrow \mathcal{P}[\varphi^{(n)}]$;
$\quad$ **if** $\|\phi^{(n+1)} - \varphi^{(n)}\| < \varepsilon$ **then**
$\quad\quad$ **return** $Id + D\phi^{(n+1)}$;
$\quad$ **end**
end

---

5. Experimental Results

In this section, we report our experimental results. More algorithmic details and results can be found in the supplementary documents.

Setup All the algorithms are developed using generic C++ compatible with Windows and Linux platforms. We mainly use libfftw [11] for Fast Fourier Transform and OpenGL, OpenCV for the user interface. All the experiments are conducted on a Windows laptop with Intel Core i7-7700HQ 2.80 GHz CPU and 16 GB memory. The surface meshes are acquired either from 3D scanning or reconstructed from medical images and represented by the half-edge data structure. All the meshes are conformally parameterized onto the unit square using surface Ricci flow algorithm [46] and resampled to the regular grids with different resolutions. The area distortion induced by the conformal mapping is called *conformal factor*.

Accuracy In order to measure the accuracy of our proposed algorithm, we implemented two metrics. Fig. 1 shows the computational example of the Budda surface with resolution 512×512, first the surface is conformally mapped onto a rectangle (c), then an OT map is calculated (d), the composition of the conformal map and the OT map is an area-
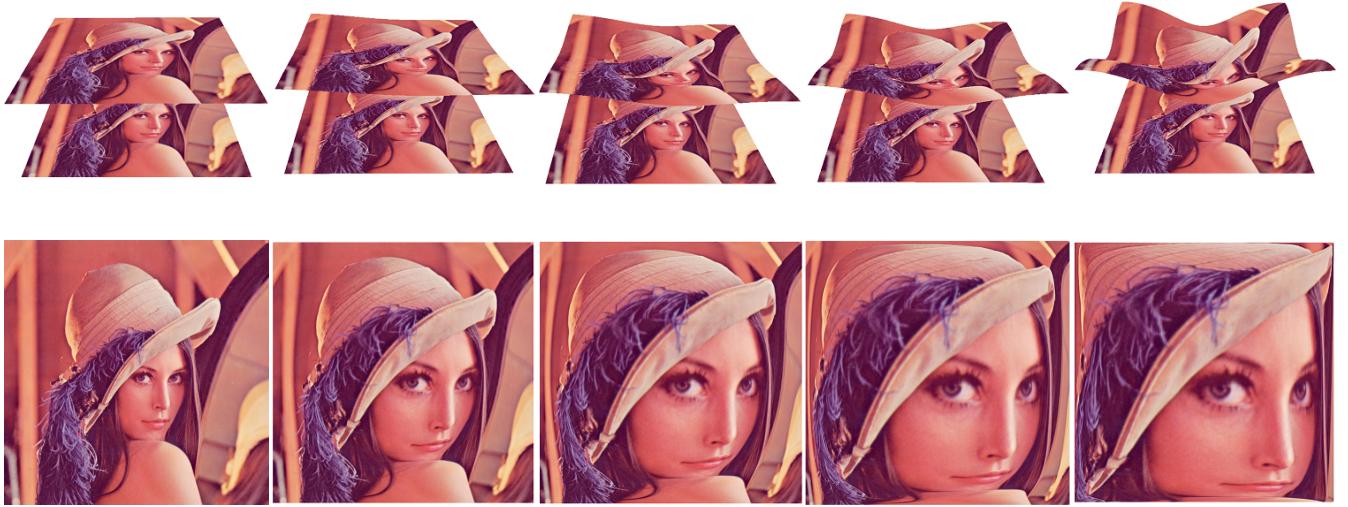
Figure 4: The iterations for the OT map from a Gaussian distribution with $\sigma_x, \sigma_y = 0.25$ and $\mu_x, \mu_y = 0$ to the Lebesgue's measure. The top row shows the Kantorovich potentials at different iterations $\varphi^{(n)}$'s, the bottom row illustrates the mappings $\mathrm{Id} + D\varphi^{(n)}$.
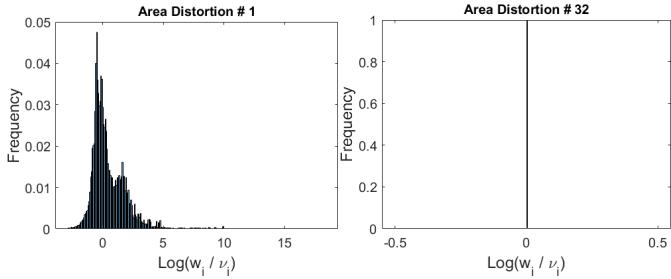

Figure 5: Accuracy Test. Historgrams of the area distortion factors on each face. Left is the initial histogram of $\varphi^{(0)}$, right is the final histogram of $\varphi^{(n)}$.

preserving map from the Budda surface to the square. For each face f_i on the mesh, we compute its original area ν_i in $\mathbb{R}^3$ and the final planar area w_i, then plot the histogram of the logarithms of the area distortion factors, $\log w_i/\nu_i$, as shown in Fig. 5. It is obvious that the final histogram highly concentrates on the origin, this shows the mapping preserves the face areas with high accuracy.

The second metric measures the solution approximation error. Suppose the resolution is $n \times n$, the discrete solution is u_n, the L^2 *approximation error* is defined as

$$E_n := \left[\int_\Omega |\mathrm{det}D^2 u_n(p) - f/g \circ Du_n(p)|^2 dp \right]^{\frac{1}{2}},$$

The right frame of Fig. 2 shows the error decreases quadratically with respect to the image resolution n, $E_n \propto 1/n^2$, hence the error can be reduced by increasing n. This numerical result is consistent with the convergence rate estimates in [5].

Efficiency In order to measure the convergence speed, we compute the L^2 distance between two adjacent intermediate Kantorovich potentials $\varphi^{(n)}$ and $\varphi^{(n-1)}$, and define the convergence error ε_n as,

$$\log \varepsilon_n := \log \left[\int_\Omega |\varphi^{(n)}(p) - \varphi^{(n-1)}(p)|^2 dp \right]^{\frac{1}{2}}.$$

The left frame of Fig. 2 shows the logarithm of ε_n during the optimization for the Buddha model, it is clear that the convergence error ε_n decreases exponentially fast with respect to n. The spacial complexity is equal to that of FFT. The recursive FFT is $O(NlogN)$, the iterative version is only $O(N)$, $N = n^2$. Here, we use the CUDA iterative FFT method.

Furthermore, we compare the proposed method with the convex geometric optimization method in [39]. Table 1 reports the comparison results for meshes with 512×512 resolution, 26144 vertices and 522242 faces; table 2 for meshes with $1k \times 1k$ resolution. The method in [39] can not handle the brain cortical surface. For the other models, the FFT-OT algorithm is tens to hundreds of times faster. The large the resolution n is, the greater the speed up factor. This demonstrates that the FFT-OT method greatly improves the computational efficiency.

Scalability The proposed FFT-OT algorithm can handle large OT problems.

In theory, the Sinkhorn method has intrinsic approximation error; in practice, it computes n^4 unknowns, therefore can't handle the $2k \times 2k$ cases in our experiments, such as the models in table 1 and table 2. The convex geometric algorithm can handle the OT problem for models with moderate complexity. If the mesh vertices exceeds one million,

the computation time will be extremely slow. In contrast, we test our proposed algorithm with different resolutions, from 512×512 upto $2k \times 2k$, the running times are reported in table 3. The experiments show that computational process is stable and scalable.

Generality Fig 7 shows an example of surface registration from the female face 9 to the male face 11 by OT maps. Both 3D surfaces are conformally mapped to the planar rectangles, then registered by the OT maps in the plane. The mappings are visualzied by warping the female face texture. The left frame shows the OT map using the texture color as densities, the right frame using the conformal factors (area distortion factors) as the densities. The method in [26, 13] assumes the target measure is uniform, therefore can't compute the registration. This shows the generality of the FFT-OT algorithm.

Simplicity The geometric variational algorithm in [40] requires dynamic geometric data structures to represent the power diagram, and adaptive/exact arithmetic libraries. During the optimization, the temporal step-length is carefully dynamically chosen to ensure the searching is inside the admissible space. Once the searching is outside the admissible space, the step-length is reduced by half recursively. The damping procedure is also used in algorithm [33] to ensure the convergence. In contrast, the FFT-OT algorithm neither has temporal step-length parameter, nor requires parameter fine tuning. Hence the proposed FFT-OT algorithm is very simple and easy to implement using OpenCV or libfftw [11]. More technical details, experimental results and source code are reported in the supplementary documents.
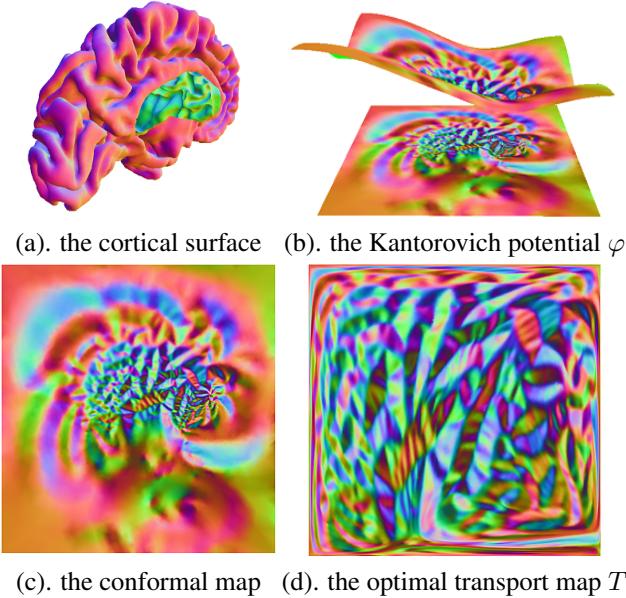

(a). the cortical surface   (b). the Kantorovich potential φ

(c). the conformal map   (d). the optimal transport map T

Figure 6: The brain cortical surface example.

Figure 7: Generality Test. Registration of the female face to the male face. Left, based on texture color; Right, based on conformal factor.
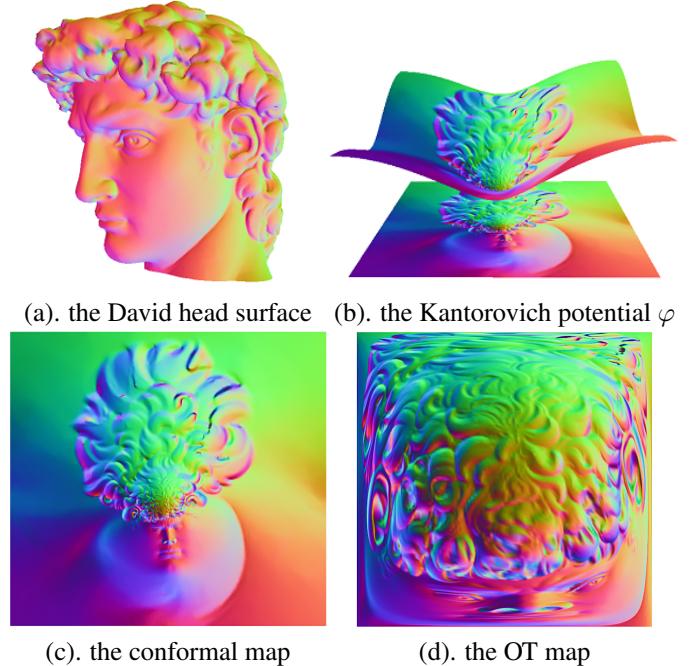

(a). the David head surface   (b). the Kantorovich potential φ

(c). the conformal map   (d). the OT map

Figure 8: The David head surface example.

Model	Fig	Su et al.(s)	FFT-OT (s)	Speedup
Buddha	1	166.293	4.24240	39.198
Brain	6	-	28.7916	-
Female	9	142.600	2.72536	52.323
Male	11	141.037	2.05898	68.498
Oldman	10	150.903	6.56181	22.997
David	8	172.514	28.338	8.482

Table 1: Efficiency Test with 512×512 resolution.

6. Conclusion

Optimal transportation plays a fundamental role in computer vision, but the computation is challenging. This work proposes a novel FFT-OT algorithm in order to improve the computational efficiency and accuracy. The key ideas are converting the optimal transportation problem to a fixed
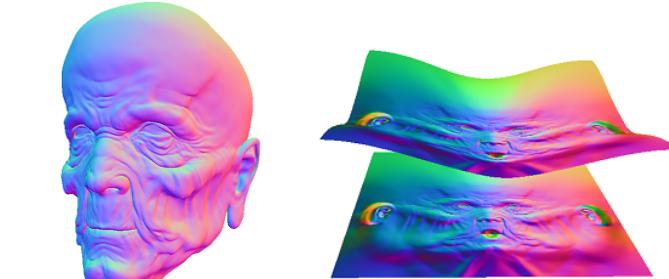
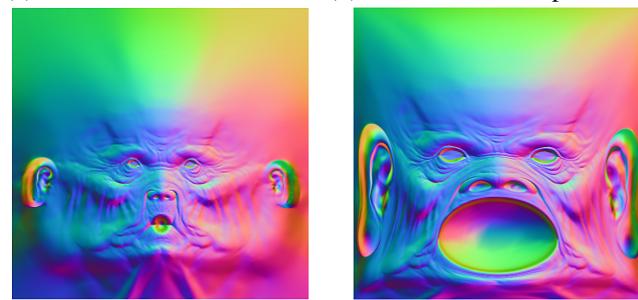(a). the female facial surface (b). the Kantorovich potential φ

(c). the conformal map (d). the OT map

Figure 9: The female facial surface example.

(a). the male facial surface (b). the Kantorovich potential φ

(c). the conformal map (d). the OT map

Figure 11: The male facial surface example.

(a). the old man head surface (b). the Kantorovich potential φ

(c). the conformal map (d). the OT map

Figure 10: The old man head surface example.

Model	Fig	Su et al.(s)	FFT-OT (s)	Speedup
Buddha	1	1200.189	11.8304	101.450
Brain	6	–	80.9929	–
Female	9	1354.564	8.0702	167.834
Male	11	1273.650	6.0111	211.883
Oldman	10	1108.373	17.8078	62.237
David	8	1391.203	80.7017	17.239

Table 2: Efficiency Testing $1k \times 1k$ resolution.

Model	Fig	512 (s)	1024 (s)	2048 (s)
Buddha	1	4.2424	11.8304	97.8272
Brain	6	28.7916	80.9929	705.6193
Female	9	2.72536	8.0702	68.6188
Male	11	2.05898	6.0111	52.5744
Oldman	10	6.56181	17.8078	149.8557
David	8	28.593	80.7017	700.1554

Table 3: Scalability Testing

In future, the FFT-OT algorithm will be generalized to handle higher dimensional situations and spherical cases for broader applications in vision and deep learning.

References

[1] Martin Arjovsky, Soumith Chintala, and Léon Bottou. Wasserstein generative adversarial networks. In *ICML*, pages 214–223, 2017. 1

[2] J.D. Benamou, Y. Brenier, and K. Guittet. The monge-kantorovitch mass transfer and its computational fluid me-

point problem, formulate the obliqueness condition as the Neumann boundary condition, and iteratively searches the solution by solving Poisson equations using FFT. The experimental results demonstrates that the FFT-OT algorithm is simple, general and scalable with high accuracy and efficiency.

chanics formulation. *International Journal for Numerical Methods in Fluids*, 2002. 1, 2

[3] J. Benamou, B. F. Hamfeldt, and A. M. Oberman. Two numerical methods for the elliptic monge-ampère equation. *ESAIM Mathematical Modelling and Numerical Analysis*, 44(4):737–758, 2010. 4

[4] Jean-David Benamou, Brittany Hamfeldt, and Adam Oberman. Two numerical methods for the elliptic monge-ampere equation. *ESAIM Mathematical Modelling and Numerical Analysis*, 44(4):737–758, 07 2010. 1, 2, 4

[5] Haodi Chen, Genggeng Huang, and Xu-Jia Wang. Convergence rate estimates for aleksandrov's solution to the monge–ampère equation. *SIAM Journal on Numerical Analysis*, 57(1):173–191, 2019. 2, 6

[6] Li Cui, Xin Qi, Chengfeng Wen, Na Lei, Xinyuan Li, Min Zhang, and Xianfeng Gu. Spherical optimal transportation. *Computer-Aided Design*, 115:181–193, 2019. 2

[7] M Cuturi. Sinkhorn distances: Lightspeed computation of optimal transportation distances. 2013, 2013. 1, 2

[8] Fernando De Goes, Katherine Breeden, Victor Ostromoukhov, and Mathieu Desbrun. Blue noise through optimal transport. *ACM Transactions on Graphics (TOG)*, 31(6):171, 2012. 2

[9] Fernando De Goes, David Cohen-Steiner, Pierre Alliez, and Mathieu Desbrun. An optimal transport approach to robust reconstruction and simplification of 2d shapes. In *Computer Graphics Forum*, volume 30, pages 1593–1602. Wiley Online Library, 2011. 2

[10] Edward J. Dean and Roland Glowinski. On the numerical solution of the elliptic monge-ampere equation in dimension two: a least-squares approach. *Partial Differential Equations, Volume 16 of Comput. Methods Appl. Sci.*, 16:43–63, 2008. 1, 2, 4

[11] Matteo Frigo and Steven G. Johnson. The design and implementation of FFTW3. *Proceedings of the IEEE*, 93(2):216–231, 2005. Special issue on "Program Generation, Optimization, and Platform Adaptation". 5, 7

[12] Aude Genevay, Marco Cuturi, Gabriel Peyré, and Francis Bach. Stochastic optimization for large-scale optimal transport. In *Advances in neural information processing systems*, pages 3440–3448, 2016. 1, 2

[13] Nader Georges and Gael Guennebaud. Instant transport maps on 2d grid. *ACM Trans. Graph.*, 37(6), 2018. 2, 7

[14] Andrew S. Glassner, editor. *Graphics Gems*. Academic Press Professional, Inc., USA, 1990. 5

[15] David Xianfeng Gu, Feng Luo, jian Sun, and Shing-Tung Yau. Variational principles for minkowski type problems, discrete optimal transport, and discrete monge-ampère equations. *Asian Journal of Mathematics*, 2016. 2

[16] Ishaan Gulrajani, Faruk Ahmed, Martin Arjovsky, Vincent Dumoulin, and Aaron C Courville. Improved training of wasserstein gans. In *NIPS*, pages 5769–5779, 2017. 1

[17] E. Haber, T. Rehman, and A. Tannenbaum. An efficient numerical method for the solution of the l2 optimal mass transfer problem. *SIAM J. Sci. Comput.*, 2010. 1, 2

[18] Steven Haker, Lei Zhu, Allen Tannenbaum, and Sigurd Angenent. Optimal mass transport for registration and warping. *International Journal of Computer Vision*, 2004. 1, 2

[19] Brittany D. Froese Jean-David Benamou and Adam M. Oberman. Numerical solution of the optimal transportation problem using the monge-ampère equation. *J. Comput. Phys*, 2014. 1, 2

[20] LV Kantorovich. On a problem of monge. *Uspekhi Mat. Nauk.*, 3:225–226, 1948. 2

[21] Leonid Vitalevich Kantorovich. On a problem of monge. *Journal of Mathematical Sciences*, 133(4):1383–1383, 2006. 2

[22] Narendra Karmarkar. A new polynomial-time algorithm for linear programming. In *STOC*, pages 302–311. ACM, 1984. 2

[23] Bruno Lévy and Erica L.Schwindt. Notions of optimal transport theory and how to implement them on a computer. *Computers & Graphics*, 72, 2018. 2

[24] Lévy, Bruno. A numerical algorithm for l2 semi-discrete optimal transport in 3d. *ESAIM: M2AN*, 49(6):1693–1715, 2015. 1, 2

[25] Tianyi Lin, Nhat Ho, and Michael I. Jordan. Greedy stochastic algorithms for entropy-regularized optimal transport problems. In *AISTATS*. 2018. 1, 2

[26] Gregoire Loeper and Francesca Rapetti. Numerical solution of the monge-amepre equation by a newton's algorithm. *Comptes Rendus Mathematique*, 340(4):319–324, 2005. 2, 7

[27] Quentin Mérigot. A multiscale approach to optimal transport. In *Computer Graphics Forum*, volume 30, pages 1583–1592. Wiley Online Library, 2011. 1, 2

[28] Takeru Miyato, Toshiki Kataoka, Masanori Koyama, and Yuichi Yoshida. Spectral normalization for generative adversarial networks. In *ICLR*, 2018. 1

[29] Saad Nadeem, Zhengyu Su, Wei Zeng, Arie E Kaufman, and Xianfeng Gu. Spherical parameterization balancing angle and area distortions. *IEEE Trans. Vis. Comput. Graph.*, 23(6):1663–1676, 2017. 1, 2

[30] Gabriel Peyré and Marco Cuturi. *Computational Optimal Transport*. https://arxiv.org/abs/1803.00567, 2018. 2

[31] Francoiss Pitie, Anil C. Kokaram, and Rozenn Dahyot. Automated colour grading using colour distribution transfer. *Computer Vision and Image Understanding*, 2007. 1

[32] J. Rabin, S. Ferradans, and N. Papadakis. Adaptive color transfer with relaxed optimal transport. In *2014 IEEE International Conference on Image Processing (ICIP)*, pages 4852–4856, 2014. 1

[33] Louis-Philippe Saumier, Martial Agueh, and Boualem Khouider. An efficient numerical algorithm for the l2 optimal transport problem with periodic densities. *IMA Journal of Applied Mathematics*, 80:135–157, June 2013. 2, 7

[34] Vivien Seguy, Bharath Bhushan Damodaran, Rémi Flamary, Nicolas Courty, Antoine Rolet, and Mathieu Blondel. Large-scale optimal transport and mapping estimation. *arXiv preprint arXiv:1711.02283*, 2017. 2

[35] Richard Sinkhorn. A relationship between arbitrary positive matrices and doubly stochastic matrices. *Ann. Math. Statist.*, 1964. 1, 2

[36] John Strain. Fast spectrally-accurate solution of variable-coefficient elliptic problems. *Proceedings of the American Mathematical Society*, 122(3):843–850, 1994. 2

[37] K. Su, L. Cui, K. Qian, N. Lei, J. Zhang, M. Zhang, and Xianfeng Gu. Area-preserving mesh parameterization for poly-annulus surfaces based on optimal mass transportation. *Computer Aided Geometric Design*, 2016. 2

[38] Zhengyu Su, Yalin Wang, Rui Shi, Wei Zeng, Jian Sun, Feng Luo, and Xianfeng Gu. Optimal mass transport for shape matching and comparison. *IEEE Transactions on Pattern Analysis and Machine Intelligence*, 2015. 1

[39] Zhengyu Su, Yalin Wang, Rui Shi, Wei Zeng, Jian Sun, Feng Luo, and Xianfeng Gu. Optimal mass transport for shape matching and comparison. *Pattern Analysis and Machine Intelligence, IEEE Transactions on*, 37(11):2246–2259, 2015. 1, 2, 3, 6

[40] Zhengyu Su, Wei Zeng, Rui Shi, Yalin Wang, Jian Sun, and Xianfeng Gu. Area preserving brain mapping. In *Proceedings of the IEEE Conference on Computer Vision and Pattern Recognition*, pages 2235–2242, 2013. 2, 7

[41] Tauseef ur Rehman, Eldad Haber, Gallagher Pryor, John Melonakos, and Allen Tannenbaum. 3d nonrigid registration via optimal mass transport on the gpu. *Medical image analysis*, 13(6):931–940, 2009. 1

[42] John I. E. Urbas. The oblique derivative problem for equations of monge-ampere type in two dimensions. *Proceedings of the Centre for Mathematics and Its Applications*, 12:171–195, 1987. 3

[43] Cédric Villani. *Topics in Optimal Transportation*, volume 58. American Mathematical Society, 2003. 2, 3

[44] Cédric Villani. *Optimal transport: old and new*, volume 338. Springer Science & Business Media, 2008. 2

[45] Xu-Jia Wang. On the design of a reflector antenna ii. *Calculus of Variations and Partial Differential Equations*, 20(3):329–341, 2004. 2

[46] Wei Zeng, Dimitris Samaras, and Xianfeng David Gu. Ricci flow for 3D shape analysis. *IEEE Transactions on Pattern Analysis and Machine Intelligence*, 32(4):662–677, 2010. 5

[47] Xin Zhao, Zhengyu Su, Xianfeng Gu, and ArieX. Kaufman. Area-preservation mapping using optimal mass transport. *IEEE Transactions on Visualization and Computer Graphics.*, 19(12):2838 – 2847, 2013. 2

[48] Xin Zhao, Zhengyu Su, Xianfeng David Gu, Arie Kaufman, Jian Sun, Jie Gao, and Feng Luo. Area-preservation mapping using optimal mass transport. *IEEE Transactions on Visualization and Computer Graphics*, 2013. 2